Mass-transport impedance at channel electrodes: accurate and approximate solutions

Thomas Holm[a,b], Mats Ingdal[a,b], Espen Fanavoll[a,b], Svein Sunde[a], Frode Seland[a], David A. Harrington[b,*]

[a] *Department of Materials Science and Engineering, Norwegian University of Science and Technology, NO-7491 Trondheim, Norway.*
[b] *Department of Chemistry, University of Victoria, Victoria, British Columbia, V8W 3V6, Canada.*

Abstract

Accurate numerical electrochemical impedance spectra at channel electrodes are obtained using commercial finite element method software. These agree with experimental measurements on the hexaammineruthenium(II/III) reversible redox couple. The numerical solutions are used as a benchmark to test the validity of some common analytical approximations for the mass-transport impedance.

Keywords: FEM, channel electrode, EIS, Leveque approximation, axial diffusion

Introduction

Improved microfluidic fabrication methods have led to a resurgence of interest in channel flow electrodes. Electrochemical impedance spectroscopy is well known as a powerful method for studying electrode processes, but the convective diffusion problem under a.c. conditions must be properly understood in order to make progress. Even for the much-studied rotating disk electrode (RDE), the convective diffusion impedance is typically modeled by approximate analytical solutions, sometimes with different expressions for high and low frequency regions [1–6], and comparison of these with numerical solutions is available, e.g., [7, 8]. Channel electrodes do not have uniform accessibility, which makes them mathematically more difficult, but there are some approximate analytical treatments [9–12]. These make one or both of the two common assumptions for channel electrodes: (1) axial diffusion (in the channel direction) can be neglected, and (ii) the Lévêque approximation applies, i.e., the velocity profile

*Corresponding author. Tel.: +1-250-721-7166
Email addresses: thomas.holm@ntnu.no (Thomas Holm), matsi@stud.ntnu.no (Mats Ingdal), espen.fanavoll@ntnu.no (Espen Fanavoll), svein.sunde@ntnu.no (Svein Sunde), frode.seland@ntnu.no (Frode Seland), dharr@uvic.ca (David A. Harrington)

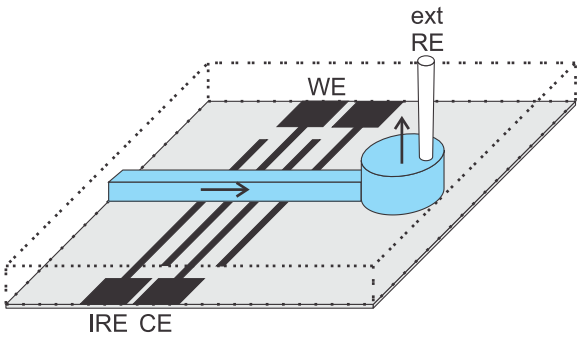

Figure 1: Diagram of the cell. Channel and outlet reservoir shown in blue, with arrows showing the fluid flow direction. IRE and ext RE are the internal and external reference electrodes.

is assumed to be linear. These are adequate only for sufficiently high channels and high flow rates. Alternatively, convection has been neglected altogether [13]. Comparisons of these approximate treatments with experiment have typically been restricted to the regimes where the approximations are valid. Experiments and theory are lacking in some important parameter regimes, in particular for low flow rates and low-height channels.

There is therefore the need for accurate numerical solutions for channel electrodes. These can be directly compared with experiment, or can be used to establish the validity of various approximate analytical methods. Both of these objectives are achieved here, where we compare numerical solutions from finite element method (FEM) software (Comsol Multiphysics®) with experiment and literature approximations, for the simple redox reaction, Eq. (1).

$$\mathrm{R} \rightleftharpoons \mathrm{P} + n\mathrm{e}^- \tag{1}$$

The experiments used the $\mathrm{Ru^{II}/Ru^{III}}$ hexammine redox couple with $n = 1$. Only a few FEM simulations of impedance have been reported before, e.g., [14, 15], none of which treat channel electrodes.

1. Methods

1.1. Microfluidics

The microfluidic flow cells, Fig. 1, were made in the NorFab facilities (Trondheim, Norway). The electrodes were prepared on clean glass slabs by a photoresist method using ma-405 photoresist and ma-D331/s developer (Micro Resist Technology GmbH). Titanium (10 nm) and platinum (190 nm) were evaporated onto the developed glass slides (Pfeiffer Vacuum Classic 500) and excess metal was removed with mr-REM 600 (Micro Resist Technology GmbH).

The PDMS channels were made from a channel master on a Si slide. The master was fabricated by applying photoresists SU8-5 and SU8-2100 (both MicroChem Corp.), developing the pattern, and removing excess material with Mr-DEV 600 (Micro Resist Technology GmbH). The wafer was then hard baked.

The PDMS was made by mixing base (Lindberg and Lund AS) and curing agent (Dow Corning S.A). The mixture was degassed and poured on top of the Si master. The finished PDMS channel was assembled by making inlet and outlet holes, activating the surface using a plasma cleaner, and then mounting on the electrode glass slide.

Wires were connected by soldering, and a reservoir for collecting the electrolyte and holding the external reference electrode was added, see Fig. 1. The cells produced had 100 μm wide electrodes in a 100 μm high channel with a depth of 1 mm.

1.2. Electrochemistry

To avoid oxygen, the microfluidic cell was mounted in a chamber that was purged with argon (Praxair Ultra High Purity 5.0). The absence of oxygen was confirmed by cycling the electrode between oxygen evolution and hydrogen evolution in 0.5 M H_2SO_4 (Seastar Chemicals, Baseline grade). Solutions were made up with Millipore Milli-Q water. All electrochemistry was performed with a Gamry Ref. 600 potentiostat. The external reference electrode used during electrochemistry in 0.5 M H_2SO_4 was a reversible hydrogen electrode mounted in the outlet reservoir, which consisted of a Pt wire sealed in glass and exposed to the solution and a trapped hydrogen bubble.

To further minimize the effect of oxygen, an iodine monolayer was deposited on the electrodes by holding at 0.4 V vs RHE for 6 minutes in 0.5 M H_2SO_4 + 4 mM KI ($\geq$ 98.5 % Caledon) electrolyte.The quality of the iodine layer was checked using cyclic voltammetry (CV) in H_2SO_4, by comparing the magnitude of the capacitive current between 0.3 and 0.7 V vs RHE. The layer was deemed sufficient if the capacitive current had dropped to below 0.01 mA cm^{-2} for a scan rate of 200 mV s^{-1}.

The data reported in this paper used the reversible Ru^{II}/Ru^{III} hexaammine redox couple. The aqueous solution was prepared from nominally 5 mM $Ru^{II}(NH_3)_6Cl_2$ ($\geq$ 98 % Sigma-Aldrich) and 5 mM $Ru^{III}(NH_3)_6Cl_3$ ($\geq$ 99.9 % Sigma-Aldrich) in 0.1 M K_2SO_4 electrolyte ($\geq$ 99.5 % AnalaR). The ruthenium hexaammine complexes degrade if there is oxygen present in the solution, and so argon was purged for 10 minutes before the complexes were introduced, and then purged again after introduction. The electrolyte was always made fresh on the day of the experiments and properly stored to avoid oxygen introduction. Despite this, slight degradation of ruthenium hexaammine did occur, and the actual concentrations were estimated as 4.0 mM by adjusting the COMSOL modeled results to give a satisfactory fit for all flow rates.

The Ru^{II}/Ru^{III} hexaammine redox couple was used as an internal reference electrode (IRE, about 0.45 V vs SHE). It was the first (most upstream) electrode in the microfluidic channel. Potentiostatic impedance spectra were collected at the Ru^{II}/Ru^{III} reversible potential as determined from the average of the anodic and cathodic peak positions in CVs. This potential was slightly offset from 0.0 V vs IRE (see Fig. 3). The ac amplitude was 5 mV (rms), and the frequency range was from 100 kHz to ca. 0.1 Hz at 20 points per decade. The lower frequency limit was chosen by noting when the impedance was not significantly changed

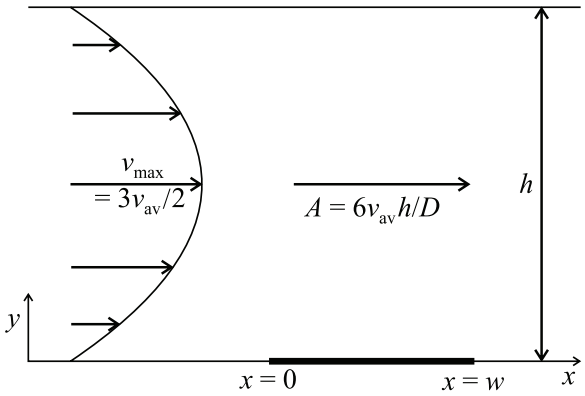

Figure 2: Geometry of the channel electrode in 2-D. Flow is from left to right, with one electrode (bold) in the bottom of the channel. The parabolic velocity profile is also shown, with the relationship between the average and maximum velocities.

on decreasing the frequency. The flow rate was varied between 1 μL min^{-1} and 300 μL min^{-1} using a syringe pump (Harvard Apparatus PHD 2000).

1.3. Modeling

The geometry modeled is shown in Fig. 2, introducing the two dimensionless parameters, A ($= 6v_{\mathrm{av}}h/D$), which is a Péclet number, and B ($= w/h$), which is a geometric parameter. Here, v_{av} is the average velocity in the channel, h is the channel height, D is a diffusion coefficient, and w is the electrode width. To model diffusional impedance on a channel electrode, one has to solve the convective-diffusion equation for a 2-D channel, Eq. (2), which assumes laminar flow with a parabolic (Poiseuille) velocity profile.

$$\frac{\partial c_i(x,y,t)}{\partial t} = D_i\frac{\partial^2 c_i(x,y,t)}{\partial x^2} + D_i\frac{\partial^2 c_i(x,y,t)}{\partial y^2} - \frac{6v_{\mathrm{av}}}{h^2}y(h-y)\frac{\partial c_i(x,y,t)}{\partial x} \quad (2)$$

Here, c_i is the concentration of reactant or product species $i = \mathrm{R}, \mathrm{P}$, and D_i is the diffusivity of species i. In the presence of the ac perturbation of angular frequency ω, the concentration will have the form of Eq. (3).

$$c_i(x,y,t) = c_{i,\mathrm{ss}}(x,y) + \tilde{c}_i(x,y)\exp(i\omega t) \quad (3)$$

Here, the ac concentration $\tilde{c}_i(x,y)$ is complex. The linearity of Eq. (2) allows the steady-state and ac problems to be separated. To force reversibility, Butler-Volmer kinetics were used with an exchange current density of 10^{15} A m^{-2}. Reversibility was verified by comparing steady-state solutions with the Nernst equation solutions at the surface. At channel walls other than the electrode, the flux was set to zero. The inlet concentration was fixed at the bulk value, and the outlet boundary condition was that the concentration gradient was zero.

The finite-element method (FEM) software Comsol Multiphysics ®[16] was used for the numerical 2-D solution of the dc and ac equations. The 2-D solution may be scaled with the electrode depth d (normal to x and y) to compare with the experimental results. Edge effects in the z direction are small for an experimental ratio of $d/h = 10$ [17]. The channel length (x-direction) was set to 20 times the electrode width to ensure that the inlet and outlet conditions did not influence the solution. The electrode started at the midpoint of the channel. A strict meshing criteria was set based on the criteria of maximum diffusion length, $x_{\max} = \sqrt{D\pi^{-1}f_{\max}^{-1}}$, where $f_{\max}$ is the maximum frequency of the modeled impedance spectrum, here 10 kHz. The electrode mesh size at the surface was set to $x_{\max}/10$, while in the electrolyte volume, the mesh was allowed to grow to $10x_{\max}$ at a growth rate of maximum 5% per mesh point. The problem was solved using the PARDISO solver including a nested dissection multi-threaded pre-ordering algorithm.

For the chosen reaction kinetics at the electrode, Comsol's impedance mode automates the solution of the ac concentrations profiles $\tilde{c}_{\mathrm{R}}(x,y)$ and $\tilde{c}_{\mathrm{P}}(x,y)$. A harmonic perturbation of the potential with an amplitude set to 5 mV was used, for frequencies between 10^{-3} to 10^{4} Hz. The steady-state potential was set to the reversible potential so the steady-state current is zero. The dimensionless convective-diffusion impedance Z/Z_0 was calculated for each frequency by numerical integration of Eq. (4), c.f. Jacobsen and West [18].

$$\frac{Z}{Z_0} = \frac{1}{w}\int_0^w \left(\frac{-\tilde{c}_{\mathrm{P}}(x,0)}{h\left(\partial\tilde{c}_{\mathrm{P}}(x,y)/\partial y\right)_{y=0}} + \frac{-D_{\mathrm{P}}\tilde{c}_{\mathrm{R}}(x,0)}{hD_{\mathrm{R}}\left(\partial\tilde{c}_{\mathrm{R}}(x,y)/\partial y\right)_{y=0}} \right) \mathrm{d}x \qquad (4)$$

This impedance may be derived using the procedure given by Orazem and Tribollet [19] (their Eq. (11.52) and following). For Butler-Volmer kinetics, Z_0 is given by Eq. (5).

$$Z_0 = 2RTh/n^2F^2D_{\mathrm{P}}d(c_{\mathrm{R}}^{\infty} + c_{\mathrm{P}}^{\infty}) \qquad (5)$$

Here F is the Faraday constant, c_i^{∞} is the bulk concentration of species i, R is the gas constant, and T is the temperature.

2. Results and Discussion

2.1. Comparison between modeled and experimental data

Cyclic voltammograms for solutions with equimolar amounts of $\mathrm{Ru^{II}}$ and $\mathrm{Ru^{III}}$ show shapes expected for a reversible couple, Fig. 3. For first cycle scans, the peak potential was independent of scan rate and the peak currents were proportional to the square root of the scan rate. The difference between anodic and cathodic peak currents in the cyclic voltammogram is due to the difference in diffusion coefficients: $D_{\mathrm{Ru^{II}}} = 8.8 \times 10^{-10}$ m^2 s^{-1}, $D_{\mathrm{Ru^{III}}} = 5.71 \times 10^{-10}$ m^2 s^{-1} [20]. The reversible potential was taken to be the average of the anodic and cathodic peak potentials, which was slightly shifted from 0.0 V vs IRE.

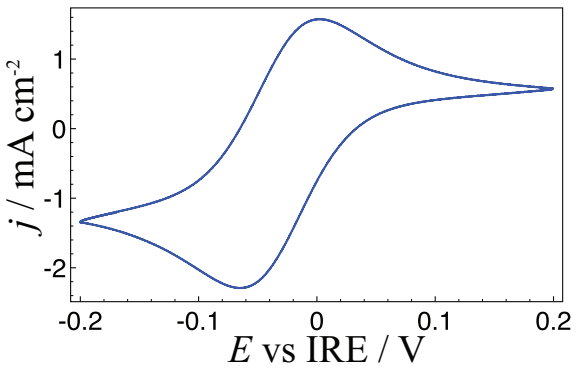

Figure 3: Steady-state cyclic voltammogram. Sweep rate 200 mV s^{-1}. No flow.

Experimental impedance spectra at the reversible potential together with numerical fits with Comsol are shown in Fig. 4 as a function of flow rate. At the highest measured frequency of 100 kHz, the impedance is essentially only real and independent of flow rate. This value represents the solution resistance. The absence of distinguishable high frequency semicircle associated with the charge transfer resistance is expected for fast reversible reaction. The observed convective diffusion impedance spectra have some features that are similar for all the flow rates. Firstly, at high frequencies (low Z values), the impedance is linear with equal values of the real and imaginary impedance. This is a well-known feature of the Warburg impedance for semiinfinite planar diffusion to the electrode. At these frequencies, the ac diffusion length is small compared to the electrode width and channel height, and senses only the stagnant layer near the electrode surface. Therefore the impedance is not influenced by convection, electrode edge effects or channel height. At lower frequencies, the impedance deviates from the linear trend and the deviation occurs at lower Z-values for higher flow rates or lower diffusivities (higher A-values), as convection becomes more important. As the ac diffusion length becomes comparable to the electrode or channel dimensions, axial diffusion and the channel height can influence the impedance. At the lowest frequencies, the concentrations and current can keep up with the sinusoidal potential changes and the impedance becomes real.

The impedance spectra were modeled as described in the Section 1.3 using the literature diffusivities quoted above, the experimental temperature of 294 K and bulk concentrations of 4 mM. The model (solid lines in Fig. 4) shows excellent agreement with the experimental results, indicating that the process is well described with the convective-diffusion equation, Eq. (2). This demonstrates the possibility of using a FE method to calculate impedance and use it as a tool to confirm the geometry or flow rate of a microfluidic flow cell.

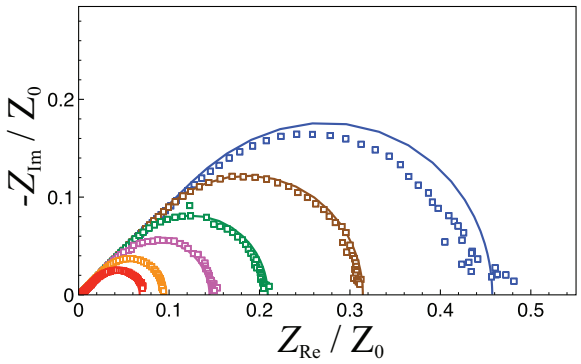

Figure 4: Potentiostatic impedance data at different flow rates. Flows in μL min^{-1} are given in the order 1 (blue), 3 (brown), 10 (green), 30 (purple), 100 (orange), 300 (red). Experimental values are the open squares. Solid lines show the Comsol results offset by the experimental solution resistance.

2.2. Comparison between numerical and analytical solutions

Analytical approximations have the advantage of simplicity over numerical simulations, but they also more easily predict parameter dependences, such as dependence of limiting currents on flow rate. Therefore the Comsol simulations were compared with two common approximations in the literature, with parameter sets chosen to match two experimental data sets with distinct A and B values. The two literature approximations for channel electrode were described in the papers by Compton and co-workers [9–11, 13]. The first method [10] simplifies the convective diffusion equation, Eq. (2), so that axial diffusion is neglected (term 2) and so that the flow is simplified as Lévêque flow (term 4), i.e., the velocity is proportional to y. The second method [13] simplifies Eq. (2) so that the convection term is neglected (term 4). Both methods assume that the diffusivities are the same for both species.

The first set of parameters is to match the above experiments, at the lowest flow rate (1 μL min^{-1}). Fig. 5 compares the experimental data (black squares) with expressions for the two approximations (evaluated in Matlab®[21]), as presented by Compton and Winkler [13]. The geometric mean of the literature diffusivities was used as the common one required by the approximations, $D = 7.089 \times 10^{-10}$ m^2 s^{-1}; other parameters are as for the experiments, leading to $A = 141.4$, $B = 1.0$. The no-convection solution (blue triangles) is far from experiment, except in the high-frequency range where the Warburg impedance for semiinfinite 1-D diffusion to a planar electrode suffices. The no-convection solution at low frequencies will only be a reasonable solution at flow rates much lower than those achieved under controlled conditions with a syringe pump. The Lévêque and no-axial diffusion approximation (green triangles) comes within the experimental error and is close to the numerical solutions. This approximation is expected to be better at higher flow rates, and so the case shown here is the most stringent test among the experimental data; higher flow rates did

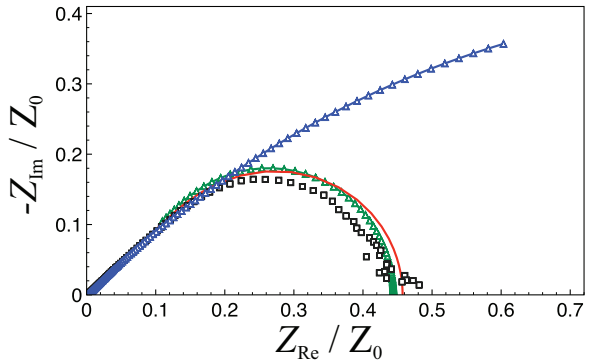

Figure 5: Potentiostatic electrochemical impedance spectroscopy modeled at a flow rate of 1 μL min^{-1}. The experimental values are shown as red squares, the Comsol model is the full line (red), the method described by Compton et al [10] assuming no axial diffusion and the Lévêque approximation for the flow is shown as the green triangles, and the solution assuming no convection is shown as blue triangles.

show better agreement between this approximation and the numerical solution. This confirms the conclusion from Compton and Winkler's work [13], that the Lévêque and no-axial diffusion approximate solution is useful for a wide range of flow conditions.

A second comparative data set is that given by Compton and Winkler [13] in their Fig. 4f, shown here as black squares in Fig. 6. Under the conditions modeled here ($A = 1234$, $B = 0.01625$), the no-convection solution (blue triangles) is not very accurate, but it is a better approximation than previously. The narrow electrodes make the Lévêque and no-axial diffusion solution (green triangles) worse than before, and so neither solution is a good approximation. Our calculated values for these approximations agree with those given by Compton and Winkler. The Comsol numerical solution of the the full convective-diffusive equation (red line) gives a result that fits well with the experimental values. Hence, for some flow conditions and geometries, it is necessary to use the full numerical solution to get a satisfactorily fit to the experimental data.

At low flow, high diffusivities, or low w/h ratios (B-values) it is expected that axial diffusion can no longer be neglected. Furthermore, the Lévêque approximation is expected to be inaccurate for wide electrodes (high B-values) or low flow rates (low A-values) as it is assumed that the top of the channel does not influence the resulting impedance. In addition, it has a high-frequency limit of applicability as derived by Compton and Sealy [10], which is normally about 50 Hz for our dimensions. This high-frequency limit is not a serious drawback, as the semiinfinite diffusion solution is a good approximation at higher frequencies.

The numerical solution clearly has advantages in the flexibility it offers for problems with all ranges of geometries and flow. Its key assumption is simply that the flow is laminar with a parabolic profile, an assumption that is well

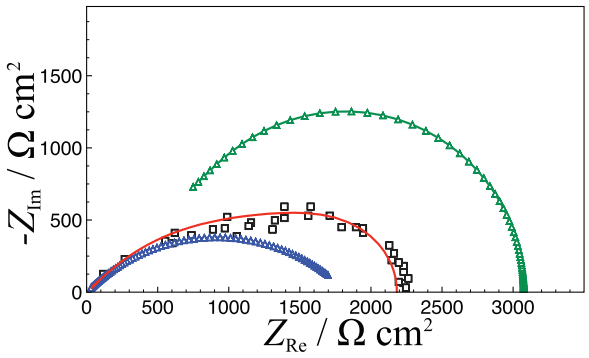

Figure 6: Model comparisons of experiment and theory. Adapted with permission from Figure 4f in Ref. [13], Copyright (1995) American Chemical Society. Experiment (red squares), Lévêque and no axial diffusion approximation (green triangles), no-convection approximation (blue triangles), Comsol numerical solution (red line).

validated in microfluidic systems some distance away from the channel inlet. The flow should not be so slow that the inlet or outlet conditions influence the result at the electrode surface, and for the numerical solution this means that at low frequencies the inlet and outlet lengths should be much longer than the ac diffusion length.

2.3. Validity of the no-axial diffusion and Lévêque approximations

Here, the solution with the Lévêque approximation and no axial diffusion is compared to the Comsol result. Assuming that Comsol gives an accurate result for all flows and geometries, the validity region for the no axial diffusion and Lévêque approximation can be determined. A matrix of values for A ($= 6v_{\mathrm{av}}h/D$), and B ($= w/h$) was simulated, and agreement between the accurate and approximate solutions was quantified based on the error at the lowest frequency. The results are color coded in Fig. 7, together with experimental values from this work (with good fit at $B = 1$, blue crosses), and from Compton and Winkler [13] ($B = 0.1$ and lower, brown crosses). Based on these results, linear zone boundaries were assigned, showing the limits of validity for the two approximations: the Lévêque approximation (dotted line, $B^{-1}A^{1/2} = 1$) and the neglect of axial diffusion (solid line, $BA^{1/2} = 3$). That is, axial diffusion may be neglected for $BA^{1/2} \geq 3$ (faster flow and wider electrodes/lower channels) and the Lévêque approximation holds for $B^{-1}A^{1/2} \geq 1$ (faster flow and narrower electrodes/higher channels). These conditions are given in terms of the original variables in Eqs. (6) and (7), and the analytical solution for no-axial diffusion and the Lévêque approximation holds when both conditions hold. If one has a geometry or flow not satisfying these conditions, a full numerical solution is necessary.

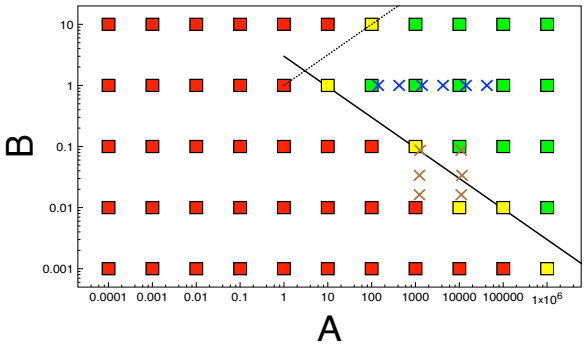

Figure 7: Validity analysis of the no axial diffusion and Lévêque approximation. Error at the lowest frequency is color coded: $< 10\%$ (green), $10-25\%$ (yellow), $> 25\%$ (red). Blue crosses are the experimental values from this work (at $B = 1$), and brown crosses are the values from Compton and Winkler's work [13] (at $B = 0.1$ and lower). The lines are the zone boundaries described in the text.

$$BA^{1/2} = \left(\frac{6w^2 v_{\text{av}}}{hD}\right)^{1/2} \geq 3 \tag{6}$$

$$B^{-1}A^{1/2} = \left(\frac{6h^3 v_{\text{av}}}{w^2 D}\right)^{1/2} \geq 1 \tag{7}$$

3. Conclusions

The FE method software (Comsol Multiphysics®) reproduces the experimental impedance spectra for a reversible redox couple, over more than two orders of magitude in flow rates. It can be used to investigate the validity of analytical methods described in the literature, namely one neglecting axial diffusion and using the Lévêque approximation for the flow, and one where the convection was neglected. Although useful for many flow regimes, the assumptions used in the derivations of these solutions are not valid for all flows and electrode sizes and the non-universal validity of these methods is demonstrated. Estimates are given for when axial diffusion can be neglected and when the Lévêque approximation holds.

The FE method can be applied for a wide set of conditions, such as flow regimes, varying diffusivities for different species, varying electrode sizes and varying kinetics. In particular, the low-frequency intercept is well determined. It has the principal drawback of numerical methods that the spectra are solved for a single set of parameters at a time, but it is promising as a guide to find more accurate analytical approximations.

4. Acknowledgements

Financial support from the Natural Sciences and Engineering Research Council of Canada (discovery grant 37035), the Research Council of Norway (project 221899), the University of Victoria, and the Norwegian University of Science and Technology is gratefully acknowledged. The Research Council of Norway is also acknowledged for the support to the Norwegian Micro and NanoFabrication Facility, NorFab (197411/V30). Thomas Holm thanks the Faculty of Natural Sciences and Technology at Norwegian University of Science and Technology for the award of a scholarship.

Bibliography

[1] R. V. Homsy, J. Newman, An Asymptopic Solution for the Warburg Impedance of a Rotating Disk Electrode, Journal of the Electrochemical Society 121 (1974) 521–523.

[2] E. Levart, D. Schuhmann, Comparison of Some Solution for the Warburg Impedance of a Rotating Disk Electrode, Journal of the Electrochemical Society 122 (1975) 1082–1083.

[3] E. Levart, J. Newman, Discussion of "The Warburg Impedance in the Presence of Convective Flow", Journal of the Electrochemical Society 127 (1980) 2649–2650.

[4] D. A. Scherson, J. Newman, The Warburg Impedance in the Presence of Convective Flow, Journal of the Electrochemical Society 127 (1980) 110–113.

[5] C. Deslouis, C. Gabrielli, B. Tribollet, An Analytical Solution of the Non-steady Convective Diffusion Equation for Rotating Electrodes, Journal of the Electrochemical Society 130 (1983) 2044–2046.

[6] B. Tribollet, J. Newman, Analytic Expression of the Warburg Imepdance for a Rotating Disk Electrode, Journal of the Electrochemical Society 130 (1983) 822–824.

[7] E. Levart, D. Schumann, Sur la determination generale du comportement transitoire d'une electrode a disque tournant soumise a une perturbation electrique de faible amplitude, Journal of Electroanalytical Chemistry and Interfacial Electrochemistry 28 (1970) 45–56.

[8] R. Morris, W. Smyrl, Rigorous Treatment of Rotating Disk Electrode Impedance Data Over the Entire Frequency Range, Journal of the Electrochemical Society 137 (1990) 406–411.

[9] B. A. Coles, R. G. Compton, The theory of EC reactions at tubular electrodes, Journal of Electroanalytical Chemistry and Interfacial Electrochemistry 127 (1981) 37–42.

[10] R. G. Compton, G. R. Sealy, The theory of the ac voltammetry of reversible electrode processes at tubular electrodes, Journal of Electroanalytical Chemistry and Interfacial Electrochemistry 145 (1983) 35–41.

[11] R. G. Compton, M. E. Laing, P. R. Unwin, AC Impedance measurements at channel electrodes the effect of convection, Journal of Electroanalytical Chemistry and Interfacial Electrochemistry 207 (1986) 309–314.

[12] J. A. Alden, R. G. Compton, Microband Electrodes of Ideal and Nonideal Geometries: AC Impedance Spectroscopy, Electroanalysis 8 (1996) 30–33.

[13] R. G. Compton, J. Winkler, Hydrodynamic Voltammetry with Channel Microband Electrodes: Alternating Current Impedance Measurements, Journal of Physical Chemistry 99 (1995) 5029–5034.

[14] Y. Hoshi, M. Ohya, I. Shitanda, M. Itagaki, Diffusion Impedance of Microband Electrode Array By FEM, in: ECS meeting abstracts of the 224th ECS meeting: 2013 Oct 27 - Nov 1; San Francisco, CA, 2686.

[15] C. Gabrielli, M. Keddam, N. Portail, P. Rousseau, H. Takenouti, V. Vivier, Electrochemical Impedance Spectroscopy Investigations of a Microelectrode Behavior in a Thin-Layer Cell: Experimental and Theoretical Studies, Journal of Physical Chemistry B 110 (2006) 20478–20485.

[16] Comsol Inc, COMSOL Multiphysics v 4.4 http://www.comsol.com, 2013. Burlington, MA.

[17] E. Kjeang, B. Roesch, J. McKechnie, D. A. Harrington, N. Djilali, D. Sinton, Integrated Electrochemical Velocimetry for Microfluidic Devices, Microfluidics and Nanofluidics 3 (2007) 403–416.

[18] T. Jacobsen, K. West, Diffusion impedance in planar, cylindrical and spherical symmetry, Electrochimica Acta 40 (1995) 255–262.

[19] M. E. Orazem, B. Tribollet, Electrochemical impedance spectroscopy, p. 185-186, John Wiley & Sons, 2011.

[20] Y. Wang, J. G. Limon-Petersen, R. G. Compton, Measurement of the diffusion coefficients of $[Ru(NH_3)_6]^{3+}$ and $[Ru(NH_3)_6]^{2+}$ in aqueous solution using microelectrode double potential step chronoamperometry, Journal of Electroanalytical Chemistry 652 (2011) 13–17.

[21] The MathWorks Inc, MATLAB R2013b http://mathworks.com/products/matlab, 2013. Natick, MA.